RSC Advances

PAPER

View Article Online
View Journal | View Issue

Cite this: *RSC Adv.*, 2015, **5**, 76919

Adhesive RAFT agents for controlled polymerization of acrylamide: effect of catechol-end R groups†

Olabode O. Oyeneye, William Z. Xu and Paul A. Charpentier*

Received 11th August 2015
Accepted 28th August 2015

DOI: 10.1039/c5ra16193b

www.rsc.org/advances

Synthesizing polyacrylamide (PAM) inorganic nanocomposites with stable tethering and controlled polymer length has been elusive. Herein, we report on the synthesis of trithiocarbonates with several catechol end R groups (as anchors) that differ in their carbonyl α-substituents. These so-called adhesive RAFT agents were subsequently examined in batch RAFT polymerization of the acrylamide (AM) monomer to study their living characteristics. The catechol-end trithocarbonates (Dopa-CTAs) and catechol-end PAM structures (≤46 kDa) were confirmed *via* 1D (^{1}H and ^{13}C) and 2D (gHSQC, gHMBC) NMR. Subsequent anchoring of the end-functionalized PAM (grafting to) *via* catechol induced linkage to γ-alumina nanoparticles was successful, giving good correlation based on ATR-FTIR, DLS and TGA analyses. This unique methodology enables PAM-inorganic nanocomposites to be synthesized with stable tethering without significant rate retardation.

Introduction

Polymeric inorganic nanocomposites (PNCs) using so-called "smart" (co)polymers[1–4] have shown potential by harnessing the synergic effects of both the polymer and inorganic components to enhance the properties for end-use applications such as water treatment flocculation.[5–7] To link the polymer component to the inorganic nanoparticles, various coupling molecules have been investigated including carboxyls,[8] catechol derivatives,[9–13] phosph(on)ates,[14] silanes,[15–17] and thiols.[18–20] Catechol derivatives have been shown to provide strong and stable chemisorption bonding between the polymer component and inorganic nanoparticles.[11–13] To provide this catechol functionality, dopamine is bifunctional with an amine moiety that can be chemically modified for amide linkage formation to polymer, while the catechol will promote mono- or bi-dentate bonding to the inorganic nanoparticles (NPs).[21,22]

Strategies commonly used for the synthesis of pre-defined PNCs involve controlled radical polymerization (CRP) using either "grafting from" or "grafting to" approaches, with the latter entailing the immobilization of end-functionalized polymer on NPs. The inorganic NPs being the core help to define the final morphology of the PNC, in conjunction with controlled polymerization to ensure uniform extension of the polymeric chains from the NP core. Of the CRP techniques, the reversible addition–fragmentation chain transfer (RAFT) polymerization method has been given immense attention for the synthesis of advanced materials. This is because of its potential for tailored materials with predetermined molecular weight (MW), complex architectures, diverse functionalities and narrow dispersity (*Đ*).[23] In particular, the RAFT polymerization technique has been shown to possess advantages over both ATRP and nitroxide techniques because of the ease of implementation and the wide range of applicable monomers (functional and non-functional), solvents and conditions. Under the "grafting to" approach, end-functionalized polymers can be prepared utilizing a RAFT agent (ZC(=S)SR) that has a Z- or R-substituent bearing the required end-group.[8,24] However, selection of the substituents needs to be suited for the specific monomer, as they influence the RAFT agent reactivity, solubility and polymerization kinetics.[25] Among the various classes of RAFT agents, trithiocarbonates are more hydrolytically stable and offer better control over polymer structure derived from more activated monomers, such as acrylamide.[26]

A number of studies have utilized a catechol moiety (as an adhesive molecule) with RAFT polymerization techniques for PNC syntheses, and catechol end-functionalization of polymers is often achieved *in situ* using catechol bearing RAFT agents for polymerization[13,27] or after polymer synthesis *via* post-modification.[28,29] However, to the best of our knowledge, no studies have attempted to compare catechol bearing RAFT agents having differing substituents at their alpha positions for the most suited livingness characteristics with respect to monomers. Herein, we investigate the influence of trithiocarbonate RAFT agents bearing the same Z group but different catechol

Department of Chemical and Biochemical Engineering, University of Western Ontario, London, ON, N6A 5B9, Canada. E-mail: pcharpentier@eng.uwo.ca

† Electronic supplementary information (ESI) available: Complementary experimental section, NMR, ATR-FTIR and UV-vis spectra; polymerization kinetic plots; and *in situ* NMR polymerization spectra. See DOI: 10.1039/c5ra16193b

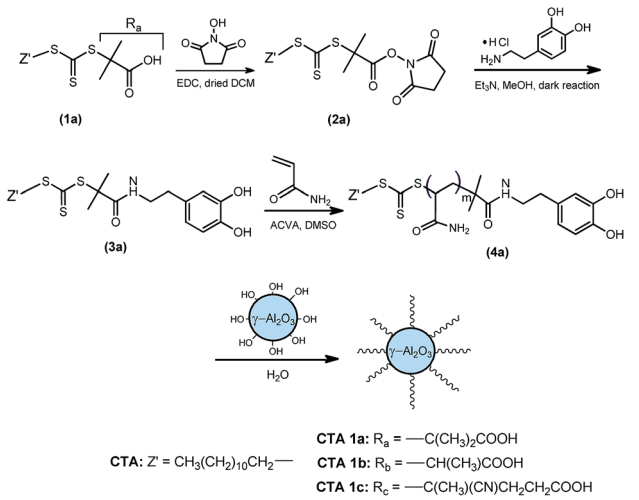

Scheme 1 End-functionalization of polyacrylamide with RAFT agents possessing different catechol-end R groups.

end R groups on acrylamide (AM) polymerization, and subsequent anchoring of the resulting polymer to γ-alumina NPs. More specifically, the catechol RAFT agents differ in the substituents on their trithiocarbonate α carbon, and one of the RAFT agents being more bulky (see Scheme 1). The catechol end R group affects the partitioning of intermediate radicals, and should be a good homolytic leaving group for preferential partitioning into new radical species (derived from the R-group) which are capable of efficient re-initiation.[30,31] We focused on end-functionalized polymers for subsequent "grafting to" as opposed to surface-initiated polymerization, because dense anchoring of the catechol-end CTA on metal oxide NPs requires conditions that cause hydrolytic decomposition of trithiocarbonate groups.[10,32] The AM monomer was chosen because of the wide utility of PAM in applications as flocculants or additives in wastewater treatment,[5,33,34] while γ-Al_2O_3 was employed because of its high OH density, high surface activity and propensity for wastewater treatment.[35,36]

Experimental section

Materials

γ-Alumina $d_{TEM} \leq 50$ nm, surface area > 40 $m^2\ g^{-1}$ (BET), acrylamide (AM, ≥98%), 4,4′-azobis(4-cyanovaleric acid) (ACVA, ≥98%), dopamine hydrochloride, *N*-hydroxysuccinimide (NHS, 98%), *N*-(3-dimethylaminopropyl)-*N*′-ethylcarbodiimide hydrochloride (EDC, ≥98%), sodium chloride (NaCl, ≥99%), 2-(dodecylthiocarbonothioylthio)-2-methylpropionic acid (DDMAT, 98%), 2-(dodecylthiocarbonothioylthio)propionic acid (DoPAT, 97%), 4-cyano-4-[(dodecylsulfanylthiocarbonyl)sulfanyl]pentanoic acid (CDSPA, 97%) and methanol (MeOH, ≥99.9%) were purchased from Sigma Aldrich, Canada and used as received. All other organic solvents used were the highest purity available from the Caledon Laboratory Ltd, Canada. Sodium bicarbonate ($NaHCO_3$, ≥95%), anhydrous sodium sulfate (Na_2SO_4, ≥99%) and anhydrous magnesium sulfate ($MgSO_4$) and sulfuric acid (96.5%) were obtained from the Caledon Labs (CA). Triethylamine (Et_3N, 99.5%) and hydrogen peroxide (30.5%) were procured from EDM Chemicals (USA). Dialysis membranes (M_W 3500 Da) were purchased from Spectrum Laboratories, Inc., while 25 μm filters (Fischer Scientific) were obtained from VWR Canada. All batch polymerization reactions were previously purged under argon atmosphere (ultra-high purity, Praxair Inc. Canada).

Characterization

A brief and detailed description of the characterization methods can be found in the ESI.†

Synthesis of RAFT agents with (2,5-dioxopyrrolidin-1-yl) oxidanyl end groups (Suc-CTAs, (2a–c))

The synthesis of Suc-CTAs was performed based on a literature method[13] by varying R groups while using a simplified workup procedure. NHS (0.40 g, 3.40 mmol) and EDC (0.76 g, 3.43 mmol) were added to 2.68 mmol each of CDSPA, DDMAT, and DoPAT dissolved in dried DCM (30 mL, previously dried with anhydrous Na_2SO_4), and allowed to react for 18 h under continuous stirring at room temperature. Each reaction mixture was then washed with 150 mL of saturated $NaHCO_3$ (aq.) before collecting the DCM phase. Further extraction from the aqueous phase was carried out with ethyl ether (5 × 30 mL), and then combined with the DCM phase to give a single organic phase, which was washed with deionized water (3 × 50 mL), brine (3 × 50 mL) and dried over anhydrous $MgSO_4$ (7.0 g). The hydrated $MgSO_4$ was filtered off and the solvent removed using a Rotavap to obtain yellowish solid products.

Suc-DDMAT. ^{1}H NMR (600 MHz, $CDCl_3$) δ (ppm): 0.89 (t, J = 7.0 Hz, 3H, $CH_3CH_2CH_2$), 1.23–1.34 (m, 16H, $CH_3(CH_2)_8CH_2$), 1.36–1.42 (m, 2H, $CH_2(CH_2)_2S$), 1.66–1.72 (m, 2H, CH_2CH_2S), 1.88 (s, 6H, $C(CH_3)_2$), 2.82 (m, 4H, (O=)C(CH_2)$_2$C(=O)), 3.31 (t, J = 7.0 Hz, 2H, CH_2S); ^{13}C NMR (100 MHz, $CDCl_3$) δ (ppm): 14.1 ($CH_3CH_2CH_2$), 22.7 ($CH_3CH_2CH_2$), 25.6 ($C(CH_3)_2$, (O=)C(CH_2)$_2$C(=O)), 27.8 (CH_2CH_2S), 29.0 ($CH_2(CH_2)_2S$), 29.1 ($CH_2(CH_2)_3S$), 29.3 ($CH_2(CH_2)_4S$), 29.4 ($CH_3(CH_2)_2CH_2$), 29.5 ($CH_3(CH_2)_3CH_2$), 29.6 ($CH_3(CH_2)_4(CH_2)_2$), 31.9 ($CH_3CH_2CH_2$), 37.2 (CH_2CH_2S), 54.3 ($C(CH_3)_2$), 168.6 (N(C=O)$_2$), 169.1 (C(=O)O), 218.7 (SC(=S)S). FTIR (cm^{-1}): 2916 ($\nu_{as}CH_2$), 2847 (ν_sCH_2), 1777 (νC=O, imide), 1734 (νC=O, ester), 1202 (νC–O, ester), 1073 (νC=S), 811 (ν_{as}S–C–S).

Suc-DoPAT. ^{1}H NMR (600 MHz, $CDCl_3$) δ (ppm): 0.88 (t, J = 7.0 Hz, 3H, $CH_3CH_2CH_2$), 1.22–1.33 (m, 16H, $CH_3(CH_2)_8CH_2$), 1.39 (quin, J = 7.2 Hz, 2H, $CH_2(CH_2)_2S$), 1.62–1.73 (m, 2H, CH_2CH_2S), 1.75 (d, J = 7.4 Hz, 3H, $CH(CH_3)$), 2.83 (br. s, 4H, (O=)C(CH_2)$_2$C(=O)), 3.37 (td, J = 7.4 Hz × 2 and 3.1 Hz, 2H, CH_2S), 5.14 (q, J = 7.4 Hz, 1H, $CH(CH_3)$); ^{13}C NMR (100 MHz, $CDCl_3$) δ (ppm): 14.1 ($CH_3CH_2CH_2$), 16.7 ($CH(CH_3)$), 22.6 ($CH_3CH_2CH_2$), 25.6 ((O=)C(CH_2)$_2$C(=O)), 27.8 (CH_2CH_2S), 28.9 ($CH_2(CH_2)_2S$), 29.0 ($CH_2(CH_2)_3S$), 29.3 ($CH_2(CH_2)_4S$), 29.4 ($CH_3(CH_2)_2CH_2$), 29.5 ($CH_3(CH_2)_3CH_2$), 29.6 ($CH_3(CH_2)_4(CH_2)_2$), 31.9 ($CH_3CH_2CH_2$), 37.5 (CH_2CH_2S), 45.0 ($CH(CH_3)$), 167.2 (N(C=O)$_2$), 168.5 (C(=O)O), 220.2 (SC(=S)S). FTIR (cm^{-1}): 2914 ($\nu_{as}CH_2$), 2848 (ν_sCH_2), 1786 (νC=O, imide), 1736 (νC=O, ester), 1471, 1358, 1200 (νC–O, ester), 1073 (νC=S), 813 (ν_{as}S–C–S).

Suc-CDSPA. ^{1}H NMR (600 MHz, *CDCl*$_3$) δ (ppm): 0.89 (t, J = 7.0 Hz, 3H, C*H*$_3$CH$_2$CH$_2$), 1.23–1.33 (m, 16H, CH$_3$(C*H*$_2$)$_8$CH$_2$), 1.35–1.44 (m, 2H, CH$_2$(CH$_2$)$_2$S), 1.66–1.73 (m, 2H, CH$_2$CH$_2$S), 1.89 (s, 3H, C(CH$_3$)), 2.48–2.69 (m, 2H, CH$_2$CH$_2$C(=O)O), 2.85 (br. s, 4H, (O=)C(CH$_2$)$_2$C(=O)), 2.94 (ddd, J = 10.0, 6.2, 3.8 Hz, 2H, CH$_2$C(=O)O), 3.34 (t, J = 7.3 Hz, 2H, CH$_2$CH$_2$S); ^{13}C NMR (100 MHz, *CDCl*$_3$) δ (ppm): 14.1 (*C*H$_3$CH$_2$CH$_2$), 22.7 (CH$_3$*C*H$_2$-CH$_2$), 24.8 (C(*C*H$_3$)), 25.6 ((O=)C(*C*H$_2$)$_2$C(=O)), 26.8 (*C*H$_2$C(=O)O), 27.6 (*C*H$_2$CH$_2$S), 28.9 (*C*H$_2$(CH$_2$)$_2$S), 29.0 (*C*H$_2$(CH$_2$)$_3$S), 29.3 (*C*H$_2$(CH$_2$)$_4$S), 29.4 (CH$_3$(CH$_2$)$_2$*C*H$_2$), 29.5 (CH$_3$(CH$_2$)$_3$*C*H$_2$), 29.6 (CH$_3$(CH$_2$)$_4$(*C*H$_2$)$_2$), 31.9 (CH$_3$CH$_2$*C*H$_2$), 33.2 (*C*H$_2$CH$_2$C(=O)O), 37.1 (CH$_2$*C*H$_2$S), 46.0 ((CH$_3$)*C*(C≡N)), 118.6 (C(*C*≡N)), 167.0 (*C*(=O)O), 168.8 (N(*C*=O)$_2$), 216.5 (S*C*(=S)S). FTIR (cm^{-1}): 2916 (ν_{as}CH$_2$), 2848 (ν_sCH$_2$), 2235 (νC≡N), 1820, 1783 (νC=O, imide), 1734 (νC=O, ester), 1423, 1383, 1293, 1199 (νC–O, ester), 1066 (νC=S), 884, 803 (ν_{as}S–C–S).

Synthesis of catechol end group CTAs (Dopa-CTAs (3a–c))

Typically, dopamine hydrochloride (0.50 g, 2.64 mmol) and each of Suc-CDSPA, Suc-DDMAT and Suc-DoPAT (2.13 mmol) were added to MeOH (30 mL) with Et$_3$N (0.40 mL, 2.87 mmol), and allowed to undergo dark reaction for 48 h at room temperature under continuous stirring. At the end of the reaction, the solvent was removed by rotary evaporation, followed by the addition of ether (20 mL) and washing of the aqueous phase. Subsequently, the ether phase was washed with deionized water (3 × 15 mL) and brine (3 × 15 mL). The ether solvent was removed by vacuum evaporation, and then the viscous solute cooled (4 °C) before precipitating in hexane (except for Dopa-CDSPA) to give a bright yellow solid product, which was vacuum dried. In the case of Dopa-CDSPA, further purification was carried out *via* preparative column chromatography using silica gel (ethyl acetate : hexane = 3 : 1 v/v).

Dopa-DDMAT. ^{1}H NMR (600 MHz, *CDCl*$_3$) δ (ppm): 0.89 (t, J = 7.0 Hz, 3H, C*H*$_3$CH$_2$CH$_2$), 1.23–1.32 (m, 16H, CH$_3$(C*H*$_2$)$_8$CH$_2$), 1.36–1.41 (m, 2H, CH$_2$(CH$_2$)$_2$S), 1.66 (s, 8H, CH$_2$CH$_2$S, C(CH$_3$)$_2$), 2.67 (t, J = 7.0 Hz, 2H, CH$_2$–ArC), 3.26 (t, J = 7.6 Hz, 2H, CH$_2$CH$_2$S), 3.41–3.49 (m, 2H, NHCH$_2$CH$_2$), 6.56 (dd, J = 8.0, 2.2 Hz, 1H, ArC–*H*(*m*-OH)), 6.64 (t, J = 5.5 Hz, 1H, N*H*CH$_2$CH$_2$), 6.71 (d, J = 2.0 Hz, 1H, ArC–*H*(*o*-OH)), 6.80 (d, J = 8.2 Hz, 1H, ArC–*H*(*o*-OH)); ^{13}C NMR (100 MHz, *CDCl*$_3$) δ (ppm): 14.1 (*C*H$_3$CH$_2$-CH$_2$), 22.7 (CH$_3$*C*H$_2$CH$_2$), 25.8 (C(*C*H$_3$)$_2$), 27.7 (*C*H$_2$CH$_2$S), 29.0 (*C*H$_2$(CH$_2$)$_2$S), 29.1 (*C*H$_2$(CH$_2$)$_3$S), 29.3 (*C*H$_2$(CH$_2$)$_4$S), 29.4 (CH$_3$(CH$_2$)$_2$*C*H$_2$), 29.5 (CH$_3$(CH$_2$)$_3$*C*H$_2$), 29.6 (CH$_3$(CH$_2$)$_4$(*C*H$_2$)$_2$), 31.9 (CH$_3$CH$_2$*C*H$_2$), 34.5 (NHCH$_2$*C*H$_2$), 37.2 (CH$_2$*C*H$_2$S), 41.7 (NH*C*H$_2$CH$_2$), 57.1 (*C*(CH$_3$)$_2$), 115.2 (Ar*C*–H(*o*-OH)), 115.4 (Ar*C*–H(*o*-OH)), 120.8 (Ar*C*–H(*m*-OH)), 130.8 (CH$_2$–Ar*C*), 142.9 (Ar*C*–OH), 144.0 (Ar*C*–OH), 173.2 (C*C*(=O)NH), 219.9 (S*C*(=S)S). FTIR (cm^{-1}): 3340 (νNH, amide), 3186 (νOH, phenol), 2920 (ν_{as}CH$_2$), 2850 (ν_sCH$_2$), 1622 and 1604 (νC=O, amide I & νC=C, aromatic), 1531 (νC–N & δNH, amide II), 1447, 1361, 1291, 1252, 1158, 1112, 1072 (νC=S), 813 (ν_{as}S–C–S).

Dopa-DoPAT. ^{1}H NMR (600 MHz, *CDCl*$_3$) δ (ppm): 0.89 (t, J = 7.0 Hz, 3H, C*H*$_3$CH$_2$CH$_2$), 1.21–1.35 (m, 16H, CH$_3$(C*H*$_2$)$_8$CH$_2$), 1.37–1.45 (m, 2H, CH$_2$(CH$_2$)$_2$S), 1.55 (d, J = 7.6 Hz, 3H, CH(C*H*$_3$)), 1.71 (quin, J = 7.5 Hz, 2H, CH$_2$CH$_2$S), 2.66 (t, J = 6.8 Hz, 2H, CH$_2$–ArC), 3.28–3.49 (m, 4H, CH$_2$CH$_2$S, NHCH$_2$CH$_2$), 4.69 (q, J = 7.6 Hz, 1H, CH(CH$_3$)), 6.50 (t, J = 5.6 Hz, 1H, N*H*CH$_2$CH$_2$), 6.57 (dd, J = 7.9, 2.1 Hz, 1H, ArC–*H*(*m*-OH)), 6.67 (d, J = 1.8 Hz, 1H, ArC–*H*(*o*-OH)), 6.80 (d, J = 8.2 Hz, 1H, ArC–*H*(*o*-OH)); ^{1}H NMR (600 MHz, DMSO-d$_6$) δ (ppm): 0.83 (t, J = 6.8 Hz, 3H, C*H*$_3$CH$_2$CH$_2$), 1.16–1.27 (m, 16H, CH$_3$(C*H*$_2$)$_8$CH$_2$), 1.28–1.35 (m, 2H, CH$_2$(CH$_2$)$_2$S), 1.42 (d, J = 7.0 Hz, 3H, CH(C*H*$_3$)), 1.60 (quin, J = 7.5 Hz, 2H, CH$_2$CH$_2$S), 2.48 (m, 2H, CH$_2$–ArC), 3.10–3.22 (m, 2H, NHCH$_2$CH$_2$), 3.33 (t, J = 7.6 Hz, 2H, CH$_2$CH$_2$S), 4.64 (q, J = 7.0 Hz, 1H, CH(CH$_3$)), 6.39 (dd, J = 7.9, 2.1 Hz, 1H, ArC–*H*(*m*-OH)), 6.54 (d, J = 2.4 Hz, 1H, ArC–*H*(*o*-OH)), 6.59 (d, J = 7.6 Hz, 1H, ArC–*H*(*o*-OH)); 8.60 (s) & 8.69 (s) (2H, Ar–OH), 8.31 (t, J = 5.6 Hz, 1H, N*H*CH$_2$CH$_2$); ^{13}C NMR (100 MHz, *CDCl*$_3$) δ (ppm): 14.1 (*C*H$_3$CH$_2$CH$_2$), 16.1 (CH(*C*H$_3$)), 22.7 (CH$_3$*C*H$_2$CH$_2$), 27.8 (*C*H$_2$CH$_2$S), 28.9 (*C*H$_2$(CH$_2$)$_2$S), 29.1 (*C*H$_2$(CH$_2$)$_3$S), 29.3 (*C*H$_2$(CH$_2$)$_4$S), 29.4 (CH$_3$(CH$_2$)$_2$*C*H$_2$), 29.5 (CH$_3$(CH$_2$)$_3$*C*H$_2$), 29.6 (CH$_3$(CH$_2$)$_4$(*C*H$_2$)$_2$), 31.9 (CH$_3$CH$_2$*C*H$_2$), 34.6 (NHCH$_2$*C*H$_2$), 37.7 (CH$_2$*C*H$_2$S), 41.3 (NH*C*H$_2$CH$_2$), 47.8 (*C*H(CH$_3$)), 115.3 (Ar*C*–H(*o*-OH)), 115.5 (Ar*C*–H(*o*-OH)), 120.7 (Ar*C*–H(*m*-OH)), 130.4 (CH$_2$–Ar*C*), 142.9 (Ar*C*–OH), 144.0 (Ar*C*–OH), 171.4 (CH*C*(=O)NH), 223.4 (S*C*(=S)S). FTIR (cm^{-1}): 3341 (νNH, amide), 3238 (νOH, phenol), 2922 (ν_{as}CH$_2$), 2848 (ν_sCH$_2$), 1633 and 1616 (νC=O, amide I & νC=C, aromatic), 1522 (νC–N & δNH, amide II), 1465, 1365, 1281, 1193, 1070 (νC=S), 813 (ν_{as}S–C–S).

Dopa-CDSPA. ^{1}H NMR (600 MHz, *CDCl*$_3$) δ (ppm): 0.89 (t, J = 6.8 Hz, 3H, C*H*$_3$CH$_2$CH$_2$), 1.22–1.34 (m, 16H, CH$_3$(C*H*$_2$)$_8$CH$_2$), 1.35–1.45 (m, 2H, CH$_2$(CH$_2$)$_2$S), 1.69 (quint, J = 7.5 Hz, 2H, CH$_2$CH$_2$S), 1.88 (s, 3H, C(CH$_3$)), 2.32–2.39 (m, 1H, CH$_2$^{a}CH$_2$C(=O)), 2.42–2.47 (m, 2H, CH$_2$CH$_2$C(=O)), 2.48–2.55 (m, 1H, CH$_2$-^{b}CH$_2$C(=O)), 2.71 (t, J = 7.0 Hz, 2H, CH$_2$=ArC), 3.33 (t, J = 7.5 Hz, 2H, CH$_2$CH$_2$S), 3.43–3.54 (m, 2H, NHCH$_2$CH$_2$), 5.63 (t, J = 5.9 Hz, 1H, N*H*CH$_2$CH$_2$), 6.61 (dd, J = 8.2, 1.7 Hz, 1H, ArC–*H*(*m*-OH)), 6.72 (d, J = 1.8 Hz, 1H, ArC–*H*(*o*-OH)), 6.83 (d, J = 8.2 Hz, 1H, ArC–*H*(*o*-OH)); ^{13}C NMR (100 MHz, *CDCl*$_3$) δ (ppm): 14.1 (*C*H$_3$CH$_2$CH$_2$), 22.7 (CH$_3$*C*H$_2$CH$_2$), 24.8 (C(*C*H$_3$)), 27.7 (*C*H$_2$CH$_2$S), 29.0 (*C*H$_2$(CH$_2$)$_2$S), 29.1 (*C*H$_2$(CH$_2$)$_3$S), 29.3 (*C*H$_2$(CH$_2$)$_4$S), 29.4 (CH$_3$(CH$_2$)$_2$*C*H$_2$), 29.5 (CH$_3$(CH$_2$)$_3$*C*H$_2$), 29.6 (CH$_3$(CH$_2$)$_4$(*C*H$_2$)$_2$), 31.9 (CH$_3$CH$_2$*C*H$_2$, *C*H$_2$C(=O)NH), 34.5 (*C*H$_2$CH$_2$C(=O)), 34.6 (NHCH$_2$*C*H$_2$), 37.1 (CH$_2$*C*H$_2$S), 41.2 (NH*C*H$_2$CH$_2$), 46.6 ((CH$_3$)*C*(C≡N)), 119.2 (C(*C*≡N)), 115.5 (Ar*C*–H(*o*-OH)), 115.7 (Ar*C*–H(*o*-OH)), 120.8 (Ar*C*–H(*m*-OH)), 130.7 (CH$_2$–Ar*C*), 142.9 (Ar*C*–OH), 144.1 (Ar*C*–OH), 171.4 (CH$_2$*C*(=O)NH), 217.2 (S*C*(=S)S). FTIR (cm^{-1}): 3286 (overlap: νNH, amide & νOH, phenol), 2919 (ν_{as}CH$_2$), 2851 (ν_sCH$_2$), 2233 (νC≡N), 1640 and 1603 (νC=O, amide I & νC=C, aromatic), 1519 (νC–N & δNH, amide II), 1442, 1360, 1280, 1193, 1151, 1112, 1065 (νC=S), 803 (ν_{as}S–C–S).

RAFT polymerization of acrylamide

All polymerization experiments were performed at 2 M monomer concentration ([M]$_0$ = 0.049 mol AM) in 24.5 mL DMSO/DMF (97 : 3, vol%) solvent (vol. of DMF is equivalent to 0.2 AM]$_0$) and 70 °C under argon atmosphere. The DMF was added as an internal reference for the determination of conversion of monomer using subsequent NMR analysis. The

initial CTA to initiator ratio ($[CTA]_0/[I]_0 = 5$) and the initial monomer to CTA ratio ($[M]_0/[CTA]_0 = 500$) were held constant to ensure controlled polymerization. AM (3.554 g, 0.049 mol), ACVA (5.6 mg, 0.0196 mmol), 24.5 mL DMSO/DMF (97 : 3 vol%) solvent and the catechol-end RAFT agent (0.098 mmol each, **3a–c**) were added to a 100 mL two-neck round-bottom flask equipped with a magnetic stirrer, and a reflux condenser was connected to one of its necks. The flask had its other neck sealed with a rubber septum through which its content was purged with argon for 20 min, before immersing the flask into an oil bath for temperature control as the experiment commenced. At predetermined intervals, 2–3 drops of samples were taken for monomer conversion analysis by ^{1}H NMR while aliquot samples were quenched immediately in liquid nitrogen and then purified prior to GPC analysis. The polymer samples were purified by three cycles of precipitating in 20 times acetone and re-dissolving in deionized H_2O before freeze-drying to obtain dried polymer. However, for NMR analysis of the structure of the synthesized polymer, further purification *via* dialysis (3500 MWCO) against distilled water was carried out.

Pre-treatment of γ-Al_2O_3 NP

Alumina NPs were pretreated by washing with acetone (twice) and immersed in piranha solution for 30 min (96.5% H_2SO_4 and 30.5% H_2O_2 (4 : 1 vol.)) to remove organic contaminants and to enhance the hydroxylation of the NP surface. Then, the NPs were extracted by washing with water and ethanol, and then vacuum dried.

Preparation of γ-Al_2O_3-PAM nanocomposite (Al-PAM)

Following ultrasonication of the pretreated alumina NP cores (30 mg), a solution containing (5 mg mL^{-1}) of Dopa-PAM (M_n = 26 500, 42 600, 53 800 g mol^{-1}; synthesized from Dopa-CTA (**3a**)) was dispersed in 15 mL deionized water at 50 °C for 24 h. Then excessive polymer was removed *via* dissolution and centrifugation before freeze-drying to obtain the dried Al-PAM nanocomposites. For preparing the control Al-PAM sample, a similar procedure was employed except that the polymer used was a PAM synthesized with CTA (**1a**) (without catechol moiety, M_n = 29 600 g mol^{-1}).

Results & discussion

Synthesis and characteristics of catechol end group RAFT agents (Dopa-CTAs (3a–c))

Though the carboxyl group of the CTAs (**1a–c**, Scheme 1) could be employed as anchor, we chose the catechol moiety because of its ability to chelate various metal oxides (HfO_2, ZrO_2, MnO_2, Y_2O_3, Al_2O_3, TiO_2, Fe_2O_3),[21,37–39] comparatively better pH stability of its complexes,[40] and the relatively mild procedure for its ligand exchange process.[8,40,41] Since the trithiocarbonate moiety of RAFT agents is known to decompose at elevated temperature,[32] Dopa-CTAs (**3a–c**) were synthesized *via* amide linkages under mild conditions (Scheme 1).[13,42] This approach involved initial coupling of carboxyl CTAs (**1a–c**) with a better leaving group (NHS) using EDC as the carboxyl activating agent before amidization. NHS esters allow efficient coupling with amines to yield amide bonds.[42] The Dopa-CTAs ((**3a–c**), termed Dopa-DDMAT, Dopa-DoPAT and Dopa-CDSPA respectively) were then prepared by reacting dopamine with NHS-activated esters of the carboxylic RAFT agents (**2a–c**). The formed compounds (**3a–c**) were confirmed *via* 1D (^{1}H and ^{13}C) and 2D (gHSQC) NMR, ATR-FTIR, and UV-vis spectroscopy.

^{1}H NMR spectra of dopamine hydrochloride, DDMAT (**1a**), Suc-DDMAT (**2a**), and Dopa-DDMAT (**3a**) are compared in Fig. 1. The spectra show all the ^{1}H peaks for the four compounds (dopamine HCl, (**1a**), (**2a**) and (**3a**)), except the weak broad carboxylic acid peak which is located at 10.73 ppm (for full spectra of DDMAT (**1a**), see ESI Fig. S1†). With DDMAT (**1a**) being converted into Suc-DDMAT (**2a**), this acid peak disappears while a new peak 29, attributed to succinimidyl protons, appears at 2.82 ppm. Further conversion of Suc-DDMAT (**2a**) into Dopa-DDMAT (**3a**) was evident by the absence of the peak 29 in the spectrum of Dopa-DDMAT (**3a**), and the presence of new peaks 17–19, 21, 22, and 25. The peak 17 is the characteristic signal for the secondary amide proton, while peaks 21, 22 and 25 are ascribed to the catechol moiety.[13,40,43] It should be noted that the ^{1}H peaks of phenol hydroxyl groups 26 and 27 were absent when using $CDCl_3$ as solvent but would show when using DMSO-d_6 as solvent. ^{13}C NMR spectra of dopamine HCl, DDMAT (**1a**), Suc-DDMAT (**2a**), and Dopa-DDMAT (**3a**) are compared in ESI Fig. S2.† The synthesized Dopa-DDMAT (**3a**) was confirmed by the shifting of the ^{13}C carbonyl peak 16 and the presence of new ^{13}C peaks 18–25 which are comparable to those of the dopamine HCl. All the correlation ^{1}H/^{13}C peaks for the synthesized Dopa-DDMAT (**3a**) are clearly shown in ESI Fig. S3,† confirming its peak assignments and molecular structure. Similarly, the conversions of (**1b**) to (**2b**) then (**3b**), (**1c**) to (**2c**) and (**3c**) were also confirmed by their ^{1}H and ^{13}C NMR spectra in (ESI Fig. S4–S7†). The synthesized Dopa-CTAs (**3a–c**) was also confirmed by ATR-FTIR investigation (ESI Fig. S8–S10†). Considering the UV wavelength range 320 to 280 nm for qualitative analysis, the trithiocarbonate group on the Dopa-CTAs (**3a–c**) was confirmed by the presence of a strong absorption peak centred at 308–310 nm (ref. 13) while a shoulder peak at 292–294 nm reveals the chromophoric effect of the 3,4-dihydroxyphenyl substituent (ESI Fig. S11–S13†).

Batch RAFT polymerization of the Dopa-CTAs

To investigate the influence of the Dopa-CTAs over the growth of catechol functionalized polyacrylamide (DPAM), RAFT polymerization of acrylamide was carried out with a ratio of $[AM]_0$: $[Dopa\text{-}CTA]_0$: $[ACVA]_0$ = 2500 : 5 : 1 at 70 °C for each of the synthesized Dopa-CTAs (**3a–c**), with the results listed in Table 1. Due to poor noise-to-catechol signal ratios as the DPAM M_w increases, the number-average M_w values *via* NMR analysis were only determined for 1 h DPAM samples and found to be comparable with GPC measurements (ESI Table S1†). The RAFT process was restricted to approximately 10 h, since the cumulative radical activity of ACVA in DMSO is known to drop drastically beyond 10 h.[26] As seen in Fig. 2a, the number-average molecular weights ($M_{n,GPC}$) of DPAMs (**4a–c**) synthesized using

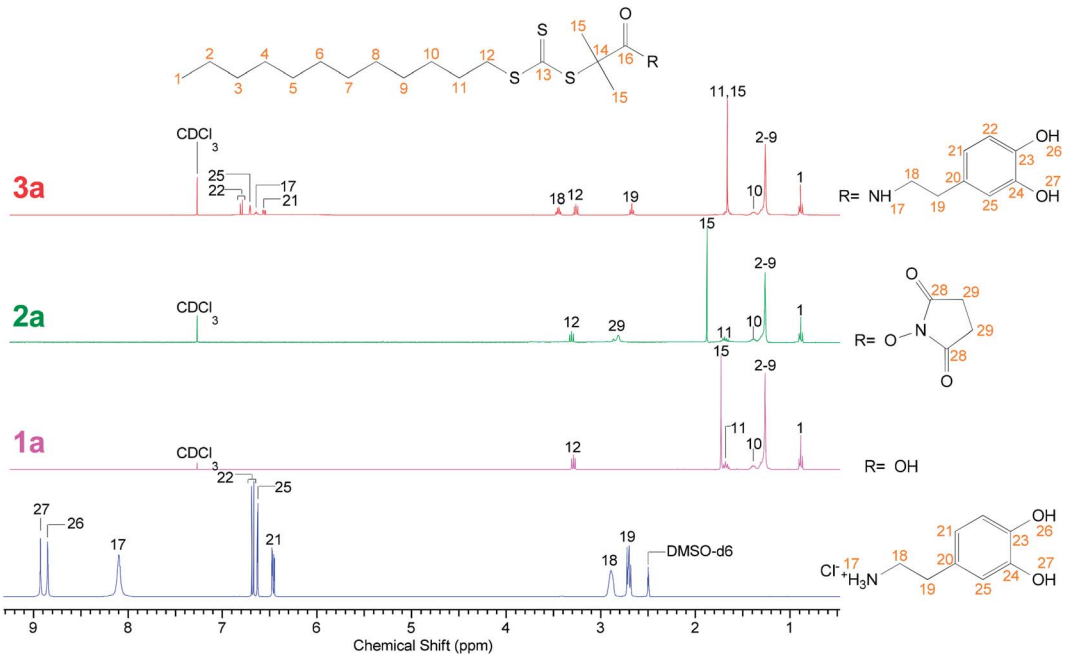

Fig. 1 ^{1}H NMR spectra of (bottom) dopamine hydrochloride, (**1a**) DDMAT, (**2a**) Suc-DDMAT, and (**3a**) Dopa-DDMAT (600 MHz, @25 °C).

Table 1 RAFT polymerization of acrylamide mediated with Dopa-CTAs[a]

Dopa-CTA (3)	Time (min)	Conv. (%)	$M_{n,GPC}$	$M_{n,the}$[b]	M_w	M_w/M_n
(**3a**)	60	35.6	14 800	13 200	17 600	1.19
	120	61.1	26 200	22 200	27 300	1.04
	240	83.0	33 700	30 000	36 100	1.07
	360	87.5	36 300	31 000	38 900	1.07
	630	93.3	40 700	33 700	42 700	1.05
(**3b**)	60	25.4	13 900	9500	16 800	1.21
	120	51.5	23 800	18 800	26 100	1.10
	240	77.3	33 100	28 000	36 500	1.10
	360	85.1	38 000	30 700	42 900	1.13
	615	89.3	41 000	32 200	45 700	1.12
(**3c**)	60	19.4	9400	7400	11 300	1.21
	120	35.6	19 600	13 200	22 100	1.13
	240	62.4	33 300	22 700	36 800	1.10
	360	72.6	42 400	26 300	45 900	1.08
	610	78.3	46 300	28 400	48 500	1.05

[a] Reaction conditions: $[AM]_0 : [Dopa\text{-}CTA]_0 : [ACVA]_0 = 2500 : 5 : 1$, solvent = 24.5 mL DMSO/DMF (97 : 3, vol%), temp. = 70 °C, $[AM]_0$ = 2 M. [b] $M_{n,the} = AM_{MW} \times P \times [AM]_0/[Dopa\text{-}CTA]_0 + [Dopa\text{-}CTA]_{MW}$ (where P is AM conversion, $P = 1 - [AM]/[AM]_0$).

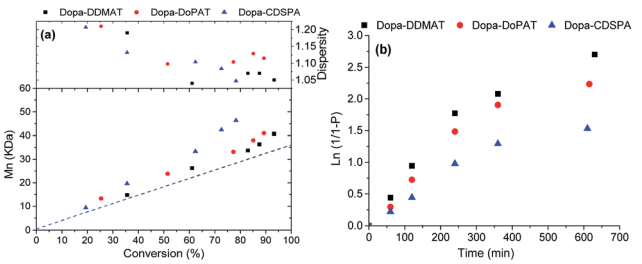

Fig. 2 RAFT Polymerization of acrylamide mediated with Dopa-CTAs (**3a–c**) using $[M]_0 : [CTA]_0 : [I]_0 = 2500 : 5 : 1$ ($[M]_0 = 2$ M), (a) evolution of molecular weight (M_n) and dispersity with conversion (the theoretical M_n is represented with broken line —); and (b) pseudo-first order kinetics, where P is AM conversion, $P = 1 - [AM]/[AM]_0$. Note: the theoretical M_n line slightly differs for each polymerization; however the lines overlap due to the insignificant difference in the MW of the Dopa-CTAs (**3a–c**).

the three Dopa-CTAs (**3a–c**) increase with increasing conversion of monomer AM while the dispersities ($Đ$) are very low, ≤1.21, showing the characteristics of living/controlled polymerization. More so, increased molecular weight was evidenced by the shift in the GPC DRI peaks toward shorter retention times (ESI Fig. S14†). Nonetheless, the number-average molecular weights ($M_{n,GPC}$) of the DPAM (**4a–c**) overshoot their predicted values ($M_{n,theo}$) with those of Dopa-CDSPA (**4c**) giving the highest overshoot (Fig. 2a). Similar overshoots have been observed in a number of studies involving polymerization of acrylamide-based monomer mediated with trithiocarbonate RAFT agents,[26,32,44] with one of the plausible reasons for such discrepancy as explained by Thomas *et al.*[26] being the limited extent of utilization of the Dopa-CTAs.

The pseudo first order kinetic plots for AM polymerization using the Dopa-CTAs shown in Fig. 2b deviate from linearity, approaching a polynomial distribution, thereby suggestive of the rate of propagation having non-steady state behaviour. This non-linearity may be explained by the change in cumulative radical production from ACVA in DMSO at 70 °C owing to its decay constant.[26] Additional details on the cumulative radical production from ACVA in DMSO solvent as related to its decomposition rate constant at 70 °C can be found in the literature.[26] More so, as identified by Moad and Barner-Kowollik,[25] the causes of non-steady state polymerization during the

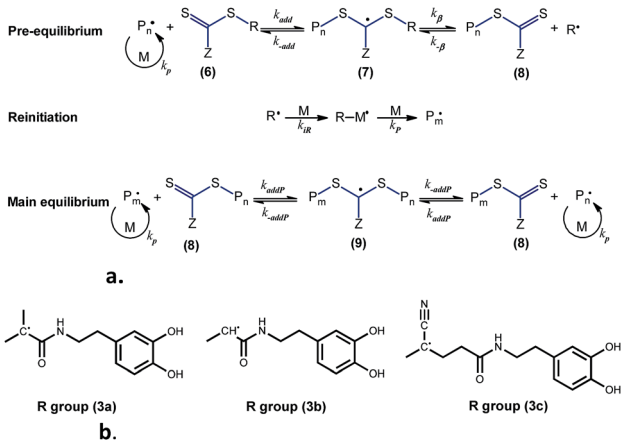

Scheme 2 (a) RAFT Equilibria. (b) R group radicals of the Dopa-CTAs (**3**).

RAFT process include changing rate coefficients with chain length, slow fragmentation of RAFT adduct and large disparity in radical addition rates with respect to monomer and CTA. Cognizant of these causes, we dislodged the effect of the latter two by monitoring the rate of propagation after the pre-equilibrium period (*i.e.* after 1 h, indicative of when the initial Dopa-CTAs had been completely consumed, Fig. 2b) to address the steady state assumption of the propagating radicals [$P_m^{\cdot}$]. Overall, the Dopa-DDMAT (**3a**) RAFT agent appears to have the most preferred living characteristics based on its comparatively lower PDI values, better linearity and lower extent of M_n overshoot (Fig. 2). This is expected since the catechol R groups must be good homolytic leaving groups and be capable of re-initiation, with the ease of the former depending on the stability of their corresponding expelled radicals (catechol R group derived).[24,45] The expelled radicals for both Dopa-DDMAT (**3a**) and Dopa-CDSPA (**3c**) are tertiary, that of Dopa-DDMAT (**3a**) is stabilized by two methyl groups and an electron donating carbonyl carbon of amide group, while the other (**3c** derived) is less stabilized owing to the electron withdrawing effect of the cyano group on its radical carbon center (see Scheme 2b). The expelled radical of Dopa-DoPAT (**3b**) is a secondary radical stabilized by a methyl and an amide carbonyl. Steric effects of the catechol R groups were contributory to the stability of their corresponding expelled radicals.[24]

Alumina-PAM nanocomposite

The synthesized DPAM (**4a**) prepared *via* RAFT polymerization ($[AM]_0 : [Dopa\text{-}CTA]_0 : [ACVA]_0 = 2500 : 5 : 1$ at 70 °C; duration = 35 min) was characterized with 1D (^1H and ^{13}C) and 2D (gHSQC, gHMBC) NMR. For the 1D NMR spectra, see ESI Fig. S15–S16.† As shown in Fig. 3 (gHSQC and gHMBC spectra), all the correlation $^1H/^{13}C$ peaks confirm the peak assignments and the molecular structure of the synthesized DPAM (**4a**). In addition to the major peaks (14, 16, and 17) of the repeating unit of polyacrylamide, a few minor peaks are present in the spectra of DPAM (**4a**). Peaks 1–12 suggest the presence of the Z′ group (CH_3–$(CH_2)_{11}$–) while peaks 19, 22–23, 25–26, and 29 indicate the presence of the corresponding R group. The aromatic peaks 25, 26, and 29 confirm the catechol moiety in the synthesized DPAM. It should be noted that the peak of trithiocarbonate carbon (13) is hardly seen in the ^{13}C and gHMBC spectra in spite of an extremely weak peak at 205 ppm which might be attributed to it. Moreover, although there is no correlation $^1H/^{13}C$ peak of carbon 3 of the Z′ group in the 2D NMR spectra, this carbon peak is clearly seen in the ^{13}C NMR spectrum at 31.9 ppm (ESI Fig. S16†). With dopamine group being chemically attached to the end of polyacrylamide chains, it was expected that the catechol moiety could induce chemisorption of the polymer onto the γ-Al_2O_3 NP *via* covalent bonding or coordination (mono- or bi-dentate bond).[12,22] The catechol group acts as the adhesive moiety for mediating the nanocomposites formation *via* the "grafting to" approach. The DPAM (**4a**) was selected for anchoring to the pre-treated γ-Al_2O_3, since Dopa-DDMAT (**3a**) appeared to be the most preferred CTAs for mediating AM polymerization based on the estimated C_{tr}^{app} and the polymerization experiments. Fig. 4 shows the ATR-FTIR spectrum of the dried γ-Al_2O_3-PAM PNC after extensive washing, compared with those of the piranha-treated alumina and DPAM (**4a**). While there is no significant peak in the spectrum of the piranha-treated γ-Al_2O_3 in the range of 1000–3500 cm^{-1}, the synthesized DPAM (**4a**) shows strong amide peaks at 3334 (asymmetric N–H stretching), 3188 (symmetric N–H stretching), 1652 (amide I C=O stretching), and 1606 cm^{-1} (amide II N–H deformation and C–N stretching) in addition to three minor peaks at 2930, 1447, and 1414 cm^{-1} due to the C–H stretching, CH_2 bending, and C–N stretching vibrations, respectively.[46] The presence of these amide and C–H peaks in the spectrum of the synthesized Al_2O_3-PAM PNC indicates successful attachment of the DPAM to the Al_2O_3 NPs.

The attachment of DPAM on the surface of γ-Al_2O_3 NPs was also confirmed by TGA and DLS. Fig. 5a compares the weight loss *versus* temperature for piranha-treated Al_2O_3 NPs and Al_2O_3-PAM nanocomposites prepared using DPAM of different

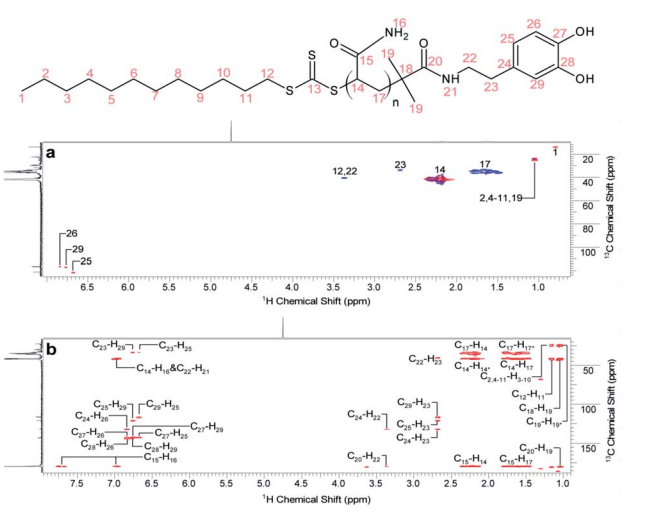

Fig. 3 2D (a) HSQC and (b) HMBC spectra of the synthesized DPAM (**4a**) in D_2O@ 25 °C. $M_{n,NMR}$ of DPAM = 9313 g mol^{-1}. * This proton is on the equivalent neighbouring carbon.

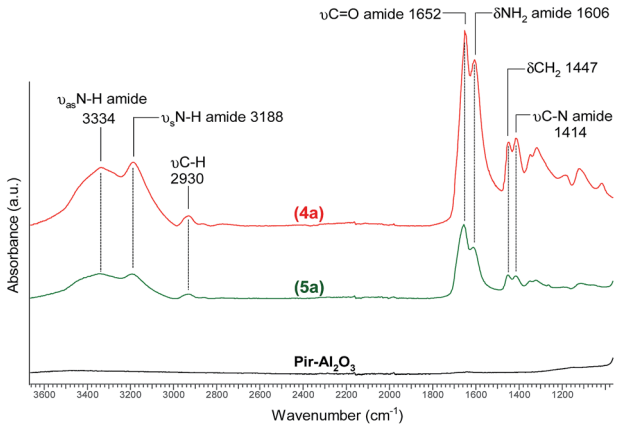

Fig. 4 ATR-FTIR spectra of piranha-treated alumina (Pir-Al_2O_3), Al_2O_3-PAM (**5a**) and DPAM (**4a**).

molecular weights and PAM (without catechol moiety, $M_{n,GPC}$ = 29 600 Da) as a control. While the piranha-treated Al_2O_3 lost 1.7% of weight when being heated to 700 °C, the control sample lost 5.7% of weight, indicating 4% of physically absorbed PAM. The Al_2O_3-PAM nanocomposites prepared using DPAM of different molecular weights (M_n = 26 200, 33 700, and 40 700 Da) demonstrated significantly high weight losses of 23.0%, 58.9%, and 73.8%, respectively. The higher sensitivity in TGA weight loss with increased MW may be due to the shorter polymer chains having enhanced interactions with the alumina NPs. The hydrodynamic size of the PNCs was assessed using the *Z*-average hydrodynamic diameter (D_h) instead of average D_h. The *Z*-average value which is based on cumulant method was used as a criterion for comparison because it is numerically stable and less sensitive to noise compared to average D_h.[47] The *Z*-average D_h values for Pir-Al_2O_3, Al_2O_3-PAM (26 200 Da), Al_2O_3-PAM (33 700 Da) and Al_2O_3-PAM (40 700 Da) were measured to be 165.8, 216.5, 233.6 and 251.5 nm, respectively, with each having a width parameter ≤0.3 (Fig. 5b). Comparison of the hydrodynamic size and PDI ($=(\sigma/d)^2$) of the Al_2O_3-PAM PNCs with the bare Pir-Al_2O_3 is indicative of good dispersivity of the PNC in water (where, σ = standard deviation, d = average diameter). As expected, the *Z*-ave size of the Al_2O_3-PAM increased with the length of the polymer chains.

This study indicates that the catechol end-group CTAs provide a suitable route for end-functionalization of PAM for post-modification chemistry. Furthermore, RAFT agents with R groups bearing catechol polar ends provide good stability for controlled polymerization.

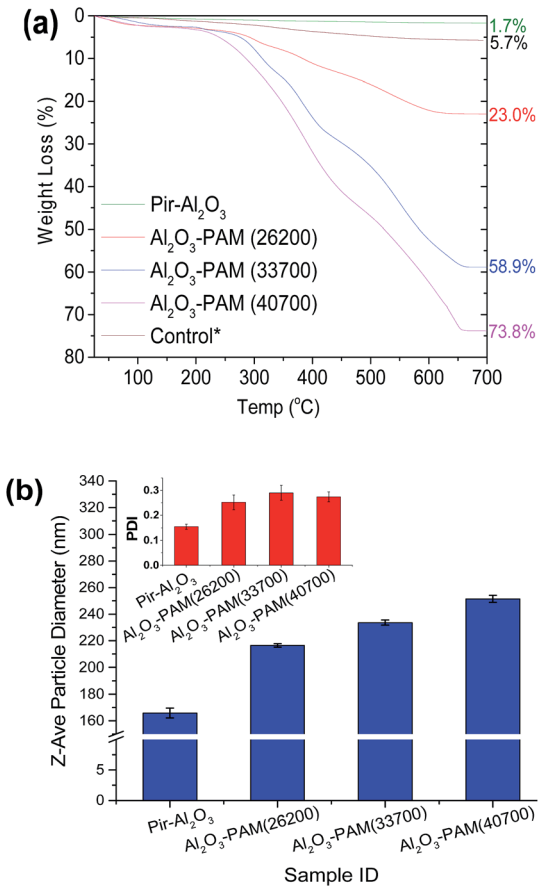

Fig. 5 Piranha-treated alumina and alumina-PAM (**5a**): (a) thermogravimetric analysis, and (b) dynamic light scattering analysis. * γ-Al_2O_3 chemisorbed with PAM (without catechol moiety, $M_{n,GPC}$ = 29 600 Da).

Conclusions

In order to produce stable tethering to metal oxide nanoparticles, three novel catechol end trithiocarbonate CTAs (Dopa-CTAs) which differ in their carbonyl α-substituents were synthesized and their molecular structures were confirmed by NMR, UV-vis and ATR-FTIR. The Dopa-CTAs were all found to mediate homo-polymerization of acrylamide in a controlled and quantitative fashion, and the Dopa-DDMAT was found to be the most preferred based on the livingness characteristics and its structural constituents. As evident from the binding studies with γ-Al_2O_3 NPs, catechol end-group CTAs provide a suitable route for end-functionalization of PAM to allow post-modification chemistry aimed at synthesizing PNCs.

Acknowledgements

The authors acknowledge Polyanalytik Inc. Ontario for providing the PEO standards used for calibrating the GPC instrument. We also thank Prof. John R. de Bruyn (Western University) and his group for granting us access to use the refractometer in their facility. Funding was provided by Canada's National Science & Engineering Research Council (NSERC) Discovery program.

Notes and references

1 Y. Wang, Y. Kotsuchibashi, Y. Liu and R. Narain, *Langmuir*, 2014, **30**, 2360–2368.
2 S. Ji and J. Y. Walz, *J. Phys. Chem. B*, 2013, **117**, 16602–16609.
3 J.-P. O'Shea, G. G. Qiao and G. V. Franks, *J. Colloid Interface Sci.*, 2011, **360**, 61–70.

4 R. Pamies, K. Zhu, S. Volden, A.-L. Kjoniksen, G. Karlsson, W. R. Glomm and B. Nystrom, *J. Phys. Chem. C*, 2010, **114**, 21960–21968.
5 H. Li, Z. Zhou, R. S. Chow and P. Contreras, *US Pat.*, 20120138543, 2012.
6 G. Rytwo, R. Lavi, Y. Rytwo, H. Monchase, S. Dultz and T. N. König, *Sci. Total Environ.*, 2013, **442**, 134–142.
7 S. Wang, M.Sc. thesis, University of Alberta, Canada, 2013.
8 B. Hojjati, R. Sui and P. A. Charpentier, *Polymer*, 2007, **48**, 5850–5858.
9 H. Lee, N. F. Scherer and P. B. Messersmith, *Proc. Natl. Acad. Sci. U. S. A.*, 2006, **103**, 12999–13003.
10 H. Lee, S. M. Dellatore, W. M. Miller and P. B. Messersmith, *Science*, 2007, **318**, 426–430.
11 E. Amstad, T. Gillich, I. Bilecka, M. Textor and E. Reimhult, *Nano Lett.*, 2009, **9**, 4042–4048.
12 W. O. Yah, H. Xu, H. Soejima, W. Ma, Y. Lvov and A. Takahara, *J. Am. Chem. Soc.*, 2012, **134**, 12134–12137.
13 C. Zobrist, J. Sobocinski, J. Lyskawa, D. Fournier, V. Miri, M. Traisnel, M. Jimenez and P. Woisel, *Macromolecules*, 2011, **44**, 5883–5892.
14 P. H. Mutin, G. Guerrero and A. Vioux, *J. Mater. Chem.*, 2005, **15**, 3761–3768.
15 C. Li and B. C. Benicewicz, *J. Polym. Sci., Part A: Polym. Chem.*, 2005, **43**, 1535–1543.
16 C. Li, J. Han, C. Y. Ryu and B. C. Benicewicz, *Macromolecules*, 2006, **39**, 3175–3183.
17 C. Yang, R. Jie, L. Jianbo and L. Yan, *Mater. Lett.*, 2010, **64**, 1570–1573.
18 C. Boyer, M. R. Whittaker, V. Bulmus, J. Liu and T. P. Davis, *NPG Asia Mater.*, 2010, **2**, 23–30.
19 B. S. Sumerlin, A. B. Lowe, P. A. Stroud, P. Zhang, M. W. Urban and C. L. McCormick, *Langmuir*, 2003, **19**, 5559–5562.
20 O. Yilmaz, M. Karesoja, A. C. Adiguzel, G. Zengin and H. Tenhu, *J. Polym. Sci. Part A: Polym. Chem.*, 2014, **52**, 1435–1447.
21 M. B. McBride and L. G. Wesselink, *Environ. Sci. Technol.*, 1988, **22**, 703–708.
22 J. H. Waite and M. L. Tanzer, *Science*, 1981, **212**, 1038–1040.
23 J. Krstina, G. Moad, E. Rizzardo, C. L. Winzor, C. T. Berge and M. Fryd, *Macromolecules*, 1995, **28**, 5381–5385.
24 L. Barner and S. Perrier, in *Handbook of RAFT polymerization*, ed. C. Barner-Kowollik, Wiley-VCH, Weinheim, 2008, pp. 455–482.
25 G. Moad and C. Barner-Kowollik, in *Handbook of RAFT polymerization*, ed. C. Barner-Kowollik, Wiley-VCH, Weinheim, 2008, pp. 51–104.
26 D. B. Thomas, A. J. Convertine, L. J. Myrick, C. W. Scales, A. E. Smith, A. B. Lowe, Y. A. Vasilieva, N. Ayres and C. L. McCormick, *Macromolecules*, 2004, **37**, 8941–8950.
27 M. Arslan, T. N. Gevrek, J. Lyskawa, S. Szunerits, R. Boukherroub, R. Sanyal, P. Woisel and A. Sanyal, *Macromolecules*, 2014, **47**, 5124–5134.
28 J. S. Kim, T. G. Kim, W. H. Kong, T. G. Park and Y. S. Nam, *Chem. Commun.*, 2012, **48**, 9227–9229.
29 Y. Min and P. T. Hammond, *Chem. Mater.*, 2011, **23**, 5349–5357.
30 D. J. Keddie, G. Moad, E. Rizzardo and S. H. Thang, *Macromolecules*, 2012, **45**, 5321–5342.
31 J. Lee, O. Kim, S. Shim, B. Lee and S. Choe, *Macromol. Res.*, 2005, **13**, 236–242.
32 A. J. Convertine, B. S. Lokitz, A. B. Lowe, C. W. Scales, L. J. Myrick and C. L. McCormick, *Macromol. Rapid Commun.*, 2005, **26**, 791–795.
33 W. Sun, J. Long, Z. Xu and J. H. Masliyah, *Langmuir*, 2008, **24**, 14015–14021.
34 W. Y. Yang, J. W. Qian and Z. Q. Shen, *J. Colloid Interface Sci.*, 2004, **273**, 400–405.
35 A. R. Barron, *Dalton Trans.*, 2014, **43**, 8127–8143.
36 B. Kasprzyk-Hordern, *Adv. Colloid Interface Sci.*, 2004, **110**, 19–48.
37 H. Gulley-Stahl, P. A. Hogan, W. L. Schmidt, S. J. Wall, A. Buhrlage and H. A. Bullen, *Environ. Sci. Technol.*, 2010, **44**, 4116–4121.
38 G. S. Tulevski, Q. Miao, M. Fukuto, R. Abram, B. Ocko, R. Pindak, M. L. Steigerwald, C. R. Kagan and C. Nuckolls, *J. Am. Chem. Soc.*, 2004, **126**, 15048–15050.
39 V. S. Wilms, H. Bauer, C. Tonhauser, A.-M. Schilmann, M.-C. Müller, W. Tremel and H. Frey, *Biomacromolecules*, 2013, **14**, 193–199.
40 H. B. Na, G. Palui, J. T. Rosenberg, X. Ji, S. C. Grant and H. Mattoussi, *ACS Nano*, 2012, **6**, 389–399.
41 H. Comas, V. Laporte, F. Borcard, P. Miéville, F. Krauss Juillerat, M. A. Caporini, U. T. Gonzenbach, L. Juillerat-Jeanneret and S. Gerber-Lemaire, *ACS Appl. Mater. Interfaces*, 2012, **4**, 573–576.
42 E. Valeur and M. Bradley, *Chem. Soc. Rev.*, 2009, **38**, 606–631.
43 A. Isakova, P. D. Topham and A. J. Sutherland, *Macromolecules*, 2014, **47**, 2561–2568.
44 M. Hernandez-Guerrero, E. Min, C. Barner-Kowollik, A. H. E. Muller and M. H. Stenzel, *J. Mater. Chem.*, 2008, **18**, 4718–4730.
45 M. L. Coote and D. J. Henry, *Macromolecules*, 2005, **38**, 1415–1433.
46 L. T. Chiem, L. Huynh, J. Ralston and D. A. Beattie, *J. Colloid Interface Sci.*, 2006, **297**, 54–61.
47 ISO. 22412:2008, *Particle size analysis – photon correlation spectroscopy*, International Organization for Standardization, Geneva, Switzerland, 2008.

